Journal of Nuclear Materials 490 (2017) 28–33

Contents lists available at ScienceDirect

Journal of Nuclear Materials

journal homepage: www.elsevier.com/locate/jnucmat

Structure and bulk modulus of Ln-doped UO_2 ($Ln = La, Nd$) at high pressure

Dylan R. Rittman [a, *], Sulgiye Park [a], Cameron L. Tracy [a], Lei Zhang [b, c], Raul I. Palomares [d], Maik Lang [d], Alexandra Navrotsky [b, c], Wendy L. Mao [a, e], Rodney C. Ewing [a]

[a] Department of Geological Sciences, Stanford University, Stanford, CA 94305, USA
[b] Peter A. Rock Thermochemistry Laboratory and NEAT ORU, University of California Davis, Davis, CA 95616, USA
[c] Department of Chemical Engineering and Materials Science, University of California Davis, Davis, CA 95616, USA
[d] Department of Nuclear Engineering, University of Tennessee, Knoxville, TN 37996, USA
[e] Stanford Institute for Materials and Energy Sciences, SLAC National Accelerator Laboratory, Menlo Park, CA 94025, USA

HIGHLIGHTS

- Ln-doped UO_2 transforms from fluorite to cotunnite at high pressure.
- Transition pressure increases with increasing hyperstoichiometry.
- Bulk modulus decreases with increasing Ln-dopant radius and concentration.

ARTICLE INFO

Article history:
Received 20 January 2017
Received in revised form
6 April 2017
Accepted 7 April 2017
Available online 10 April 2017

ABSTRACT

The structure of lanthanide-doped uranium dioxide, $Ln_xU_{1-x}O_{2-0.5x+y}$ ($Ln = La, Nd$), was investigated at pressures up to ~50–55 GPa. Samples were synthesized with different lanthanides at different concentrations ($x \sim 0.2$ and 0.5), and all were slightly hyperstoichiometric ($y \sim 0.25$–0.4). *In situ* high-pressure synchrotron X-ray diffraction was used to investigate their high-pressure phase behavior and determine their bulk moduli. All samples underwent a fluorite-to-cotunnite phase transformation with increasing pressure. The pressure of the phase transformation increased with increasing hyperstoichiometry, which is consistent with results from previous computational simulations. Bulk moduli are inversely proportional to both the ionic radius of the lanthanide and its concentration, as quantified using a weighted cationic radius ratio. This trend was found to be consistent with the behavior of other elastic properties measured for Ln-doped UO_2, such as Young's modulus.

1. Introduction

UO_2 is the dominant fuel used in nuclear reactors throughout the world. Fission of ^{235}U produces a wide variety of other elements, a major portion of which are lanthanides [1]. Off-normal conditions can expose the fuel to oxidizing conditions, leading to excess oxygen incorporation into the fuel [2]. Changes in chemistry from fission product production and oxidation can substantially influence the properties of fuel, including thermal transport, microstructure, and radiation response, especially at high burnups [3–6]. Thus, it is important to understand how the incorporation of lanthanides and oxygen interstitials into UO_2 affect its structure under extreme conditions.

UO_2 forms in the fluorite structure at ambient conditions, which consists of a face-centered cubic cation sublattice where the cations are in cubic coordination by eight anions. The anion sublattice is simple cubic, and the anions reside in tetrahedral sites within the cation sublattice. Larger Ln^{3+} substitutes for smaller U^{4+} in the fluorite structure, causing localized strain in the structure, and creating oxygen vacancies as a charge compensation mechanism. Oxidation of Ln-doped UO_2 is counterbalanced by an increase in uranium oxidation state, typically ascribed to the creation of U(V) [7–9]. Oxidation above an oxygen-to-metal (O/M) ratio of two causes some oxygen to reside in interstitial sites in the fluorite structure. Though the exact local configuration of the oxygen defect structure is still subject to debate [10,11], the fluorite structure

---

* Corresponding author.
E-mail address: drittman@stanford.edu (D.R. Rittman).

http://dx.doi.org/10.1016/j.jnucmat.2017.04.007

provides ample room for oxygen interstitials in the uranium octahedron along the [100] direction [10,12]. The fluorite structure is shown in Fig. 1a, with the positions of oxygen interstitials indicated.

The behavior of UO_2 at high pressure has generated much interest. Changing pressure, a fundamental thermodynamic variable, can assist in understanding the behavior of UO_2 by exploring the relationship between defects and structure. UO_2 transforms to the orthorhombic cotunnite-type structure (*Pnma*) at high pressure, though the pressure of this phase transformation has been debated [13–15]. In contrast to the fluorite phase, the cotunnite structure has little room for oxygen interstitials. Computational studies have indicated that this can cause substantial increases in transition pressure when starting with a hyperstoichiometric oxide. The cotunnite structure is shown in Fig. 1b, with positions of the oxygen interstitials indicated.

The elastic properties of UO_2 have been of interest for decades [16–19] since they are a determining factor in the material's mechanical properties [20] and the material's response to ion irradiation [21]. Since lanthanides are a major fission product, the effects of Ln-doping on elastic properties of UO_2 has been the subject of many studies [22–26]. High pressure allows for the determination of bulk modulus, which to date has not been investigated experimentally for Ln-doped UO_2.

Here, we conducted *in situ* high-pressure synchrotron X-ray diffraction studies on well-characterized Ln-doped UO_2 (Ln = La, Nd) [27] to understand how lanthanide-doping and hyperstoichiometry affects the structural and elastic properties of UO_2.

2. Experimental methods

Samples of polycrystalline $Ln_xU_{1\text{-}x}O_{2\text{-}0.5x+y}$ (Ln = La, Nd) were prepared with the goal of synthesizing samples with dopant levels of $x = 0.2$ and $x = 0.5$ and O/M ratio = 2 ($y = 0.5x$). However, precise control of the O/M ratio is difficult in tandem with lanthanide doping. The samples used here have accurately measured degrees of hyperstoichiometry and levels of Ln-doping (see Table 1). The investigation of several samples with varying dopant size (larger La and smaller Nd), dopant concentration, and oxygen content allows for the effects of each material parameter to be characterized and distinguished. Detailed information on the procedure for sample synthesis is provided in Ref. [27].

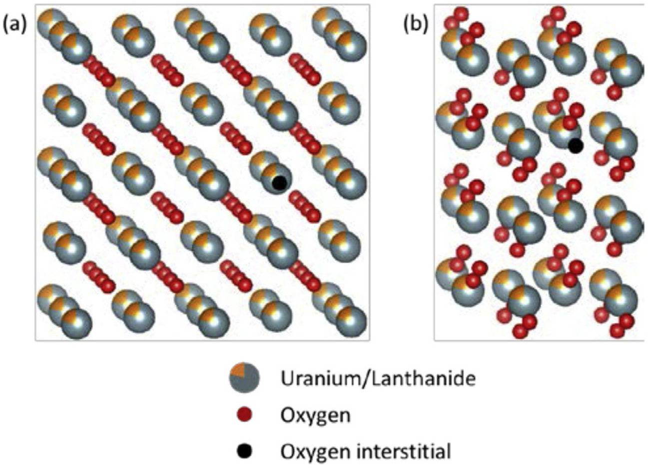

Fig. 1. Structures (2 × 2 x 2) of hyperstoichiometric Ln-doped UO_2. (a) The low-pressure fluorite phase; (b) the high-pressure cotunnite phase. Lanthanides (orange) and uranium (gray) share a site. Equilibrium oxygen positions are shown in red. Interstitial oxygen positions are shown in black. Both structures are viewed slightly off of the [010] direction. (For interpretation of the references to colour in this figure legend, the reader is referred to the web version of this article.)

Table 1
Abbreviations used for the samples along with their precise compositions, fluorite-to-cotunnite phase transformation onset pressure (P_{trans}), and bulk modulus (B_0) from a second-order Birch-Murnaghan equation of state.

Sample name	Composition	P_{trans} [GPa]	B_0 [GPa]
UO2	UO_2	30 (2)	265 (5)
Nd2	$Nd_{0.196}U_{0.804}O_{2.285}$	39 (2)	245 (5)
Nd5	$Nd_{0.507}U_{0.493}O_{2.002}$	23 (2)	193 (5)
La2	$La_{0.206}U_{0.794}O_{2.158}$	21 (2)	245 (5)
La5	$La_{0.465}U_{0.565}O_{2.116}$	29 (2)	210 (5)

High pressure was generated using diamond anvil cells (DACs), which compress materials between two opposing diamonds culets. The DACs used here had a 300 μm diameter diamond culet. A stainless steel gasket was used as a sample chamber. The gasket was pre-indented by the diamonds to thickness of 25 μm. A 120 μm hole was then drilled into the center of the pre-indention, into which the sample and pressure-transmitting medium were loaded. Pressure was determined by monitoring the fluorescence of ruby balls placed in the center of the sample chamber [28]. Error in the ruby measurement due to broadening of the fluorescence signal is ~2 GPa above 40 GPa, but is otherwise less than 0.5 GPa. Pressure was measured before and after data were collected, with the average value used as the quoted pressure. All high-pressure data were collected upon increasing pressure. Silicone oil—EDM 185™ from Commonwealth Oil—was the pressure-transmitting medium. The non-hydrostaticity of silicone oil is relatively low below 12 GPa [29].

In situ angular dispersive X-ray powder diffraction data were collected at beamline 16 BM-D of the Advanced Photon Source (APS), Argonne National Laboratory (ANL) and beamline 12.2.2 at the Advanced Light Source (ALS), Lawrence Berkeley National Laboratory (LBNL) using X-ray energies of 29.2 keV (λ = 0.4246 Å) and 25 keV (λ = 0.4959 Å), respectively. CeO_2 was used for calibration of sample position, tilt, and rotation, as well as sample-to-detector distance. Integration of two-dimensional diffraction images into diffraction patterns was performed using Dioptas [30]. Peak indexing of the integrated diffraction patterns was performed using Maud [31] in order to determine the unit cell parameters of the UO_2 phases.

3. Results and discussion

X-ray diffraction data in Fig. 2 show that all starting samples have the expected fluorite structure and undergo a high-pressure phase transformation to the orthorhombic *Pnma* cotunnite structure, consistent with the behavior of pure UO_2 [14]. The cubic *Pa-3* and orthorhombic *Pbca* structures observed in natural UO_2 at simultaneous high pressure and high temperature [32] could not be indexed to the diffraction patterns. The fluorite-to-cotunnite transformation is first evident in the appearance of multiple weak cotunnite peaks between the (111) and (200) fluorite structure peaks. The pressures corresponding to the onset of the transformation (P_{trans}) are listed in Table 1. Errors in P_{trans} result from the size of the pressure step between the pure fluorite phase and the mixed phase regimes in the X-ray diffraction data. No sample completely transformed to cotunnite at the highest pressures studied, ~50–55 GPa, and all samples fully reverted to the fluorite structure upon quenching to ambient pressure.

Fig. 3 shows the transition pressure as a function of hyperstoichiometry, defined by y in the chemical formula $Ln_xU_{1\text{-}x}O_{2\text{-}0.5x+y}$ [27]. A strong, positive correlation was found between hyperstoichiometry and P_{trans}. For this correlation to hold,

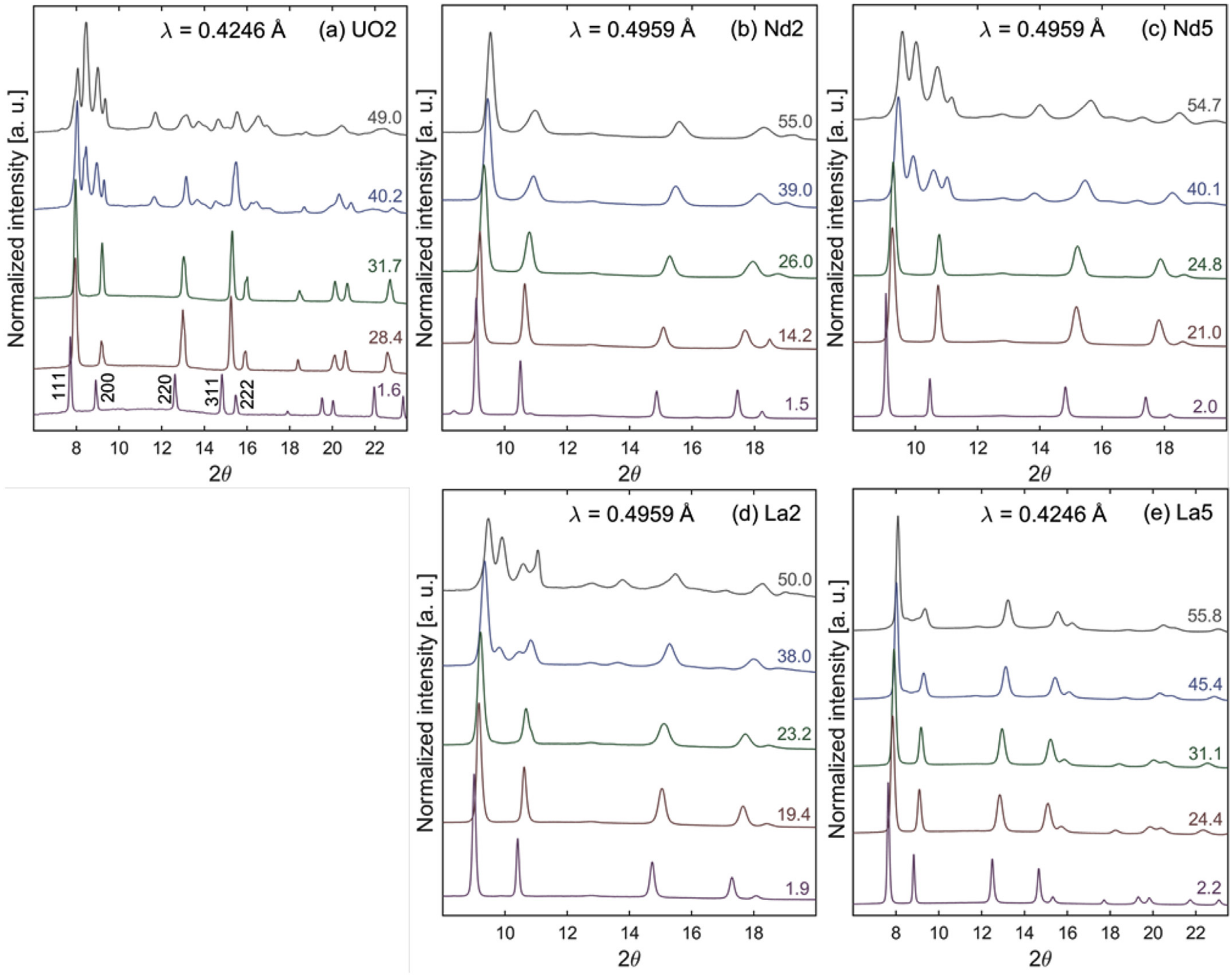

Fig. 2. Representative high-pressure X-ray diffraction patterns for all compositions. Pressures are listed to the right in GPa. The indexed peaks of the fluorite structure are shown in the lowest pressure UO_2 diffraction pattern. Transformation from fluorite-to-cotunnite is first evidenced by an increase in scattering intensity between the (111) and (200) fluorite diffraction maxima.

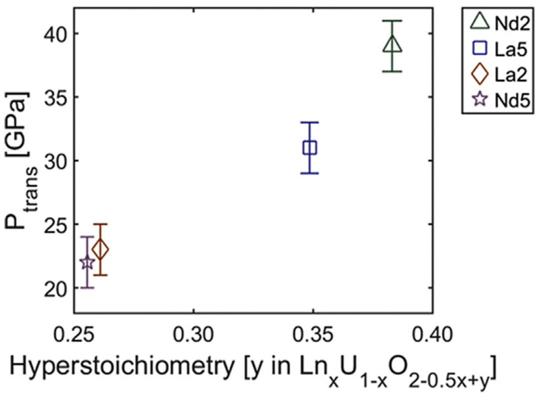

Fig. 3. Transition pressure for the fluorite-to-cotunnite phase transformation in Ln-doped samples as a function of hyperstoichiometry, defined by y in $Ln_xU_{1-x}O_{2-0.5x+y}$. Transition pressure increases as a function of increasing hyperstoichiometry. Errors in P_{trans} result from the size of the pressure step between the pure fluorite phase and the mixed phase regime in the X-ray diffraction data.

hyperstoichiometry had to be defined as y as opposed to simply the increase in O/M above 2.00. This suggests that the local structure of Ln-doped UO_2 cannot simply be thought of as Ln substituting for U within the fluorite structure. There are likely different oxygen co-ordinations depending on cation species (Ln *vs.* U), which only becomes more complex as U takes on multiple oxidation states upon doping [7–9]. Furthermore, recent neutron total scattering experiments has shown that fluorite-structured materials can have more complex short-to-medium range order: UO_2 was shown to have a local cubic *Pa-3* structure [33], and various two-cation defect-fluorite structured materials were shown to be composed of incommensurate orthorhombic *Ccmm* structural units [34]. Overall, the definition of hyperstoichiometry in Fig. 3 is consistent with the complexities involved in the local ordering of these materials.

Notably, no significant correlation was found between P_{trans} and dopant species or concentration, indicating that hyperstoichiometry affects the pressure required to induce the phase transformation much more than the structural changes caused by the incorporated lanthanide. Increasing P_{trans} with hyperstoichiometry was predicted by computational work, which showed that increasing the O/M ratio from 2.00 to 2.03 in UO_{2+x} raised the transition pressure from ~18 to ~27 GPa (~50%) [15]. The interstitial oxygen act as a large additional thermodynamic barrier to the creation of the cotunnite phase. In the fluorite structure, the vacant octahedral site provides ample room for oxygen interstitials. As such, formation of an oxygen interstitial in fluorite-structured UO_2 is energetically favorable [12]. In contrast, the cotunnite phase is more densely packed due to the ~7% volume collapse, and cannot easily incorporate oxygen interstitials. Based on computational studies, hyperstoichiometry is predicted to significantly increase the enthalpy of the transformation from fluorite to cotunnite, assuming constant stoichiometry upon compression [15].

Previous work [27] has shown that unit cell volumes in $Ln_xU_{1-x}O_{2-0.5x+y}$ are affected by both dopant and hyperstoichiometry. The effect of cation doping is explained through Vegard's law, while hyperstoichiometry has been shown to decrease unit cell volume in UO_{2+x} [35,36]. Within the $Ln_xU_{1-x}O_{2-0.5x+y}$ system, the lanthanide species and its concentration has more of an effect on unit cell volume than hyperstoichiometry [27]. High-pressure X-ray diffraction data allowed for the determination of the unit cell parameters of both the fluorite and cotunnite structures in the mixed-phase regime. Indexing of peak positions was completed on samples UO2, La2, and Nd5 since the cotunnite signal in those samples was intense enough to allow for a reliable determination of unit cell parameters. The ratio of the cotunnite unit cell parameters (a_c, b_c, c_c) to the fluorite unit cell parameter (a_f) is plotted in Fig. 4, along with the relative volume of the two phases (V_c, V_f). These ratios in Fig. 4 are the same for all samples. Thus, regardless of the lanthanide present or its concentration, the fluorite-to-cotunnite phase transformation behaves very similarly. This indicates that lanthanide doping, which dictates unit cell volume in the ambient-pressure fluorite phase, also dictates unit cell volume in the high-pressure cotunnite phase. Furthermore, a speculative interpretation of these data would be that they support the hypothesis that there are no cation site preferences in the cotunnite structure [37], and there is no clustering of lanthanides.

Pressure-volume data are plotted for the fluorite phase of all samples in Fig. 5 along with fits using a second-order Birch-Murnaghan equation of state [38]. Values of the high-pressure unit cell volumes are given in Supplementary Table S1. Data up to 12 GPa were used for the Birch-Murnaghan fit since it is the maximum pressure at which the silicone oil pressure-transmitting medium is still approximately hydrostatic [29]. A second-order fit was used because holding the pressure-derivative of bulk modulus (B′) constant allowed for direct comparison of bulk modulus (B_0) values between samples (see Table 1). Zero-pressure volumes used for the fits were based on the extrapolation of high-pressure data. Ambient-pressure X-ray diffraction measurements confirmed that these extrapolated values differed from true ambient values by less than 0.4% for all samples, independently confirming the goodness of the fits. The use of silicone oil as a pressure-transmitting medium has been shown to overestimate the bulk modulus of UO_2 [14,39]. However, the consistent use of this pressure-transmitting medium for all samples still allows for direct comparisons of the different compositions. A decrease in bulk modulus was observed for increasing dopant concentration, with the smaller Nd-doped sample experiencing a larger decrease than the larger La-doped sample.

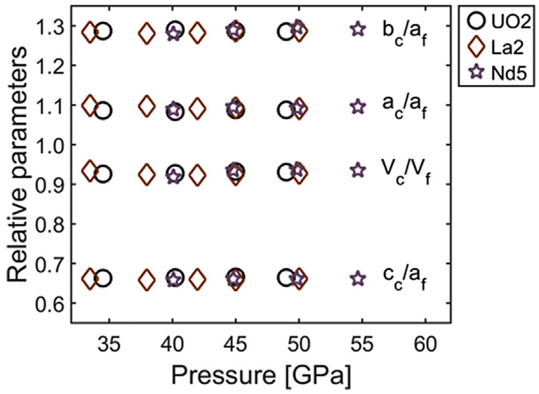

Fig. 4. Unit cell parameters and volume of the high-pressure cotunnite phase relative to the unit cell parameter and volume of the fluorite phase at various pressures. Only samples and pressure points with a high phase fraction of cotunnite were used in order to assure the accuracy of the peak indexing.

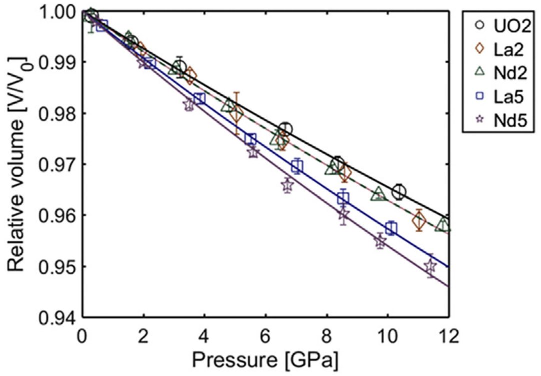

Fig. 5. Pressure-volume relation for all samples. Symbols indicate data points. Lines are fits to the second-order Birch-Murnaghan equation of state. Bulk modulus values are listed in Table 1. Errors are based on positional variations in diffraction maxima within a single XRD pattern.

This trend in bulk modulus is consistent with experiments on similarly structured (pyrochlore and defect-fluorite) two-cation cubic oxides [37,40] and computational studies of Ln-doped UO_2 [41]. To take into account both dopant species and concentration, a weighted cationic radius ratio was calculated. Equation (1) gives the weighted cationic radius ratio (w_{rr}) as a function of Ln radius (r_{Ln}), U radius (r_U), and dopant concentration (x).

$$w_{rr} = \frac{x \cdot r_{Ln}}{((1-x)\cdot r_U)} \tag{1}$$

The U radius was calculated by assuming all Ln and O were in the +3 and −2 oxidation states, respectively. It was assumed that all oxidized U prefers to be in the +5 oxidation state, though the creation of some U^{6+} was required to maintain charge balance in some samples. The precise stoichiometries in Table 1 allowed the proportions of U^{4+}, U^{5+}, and U^{6+} to be calculated through charge balance considerations. Shannon radii [42] were used for all atoms, and it was assumed that all cations were eight-coordinated by oxygen. Changes in coordination from the excess oxygen is possible, which would slightly alter the radii. However, there is much debate surrounding the positions of interstitial oxygen in UO_2 [10,11], so the exact coordination could not be determined. B_0 values as a function of weighted cationic radius ratio are plotted in Fig. 6 along with the linear fit to the data. It should be noted that satisfactory linear fits to the data were obtained using (1) different U oxidation behavior, and (2) a variety of ionic radii that could reasonably occur in other oxygen coordination schemes, indicating that the assumptions made here do not greatly affect the analysis. Samples with a larger cation size mismatch result in a lower bulk modulus, indicating that microstrain caused by structural

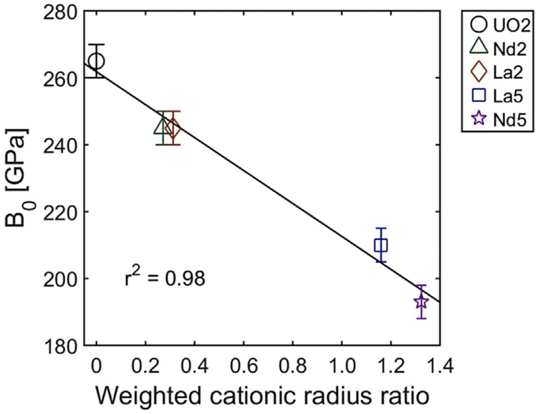

Fig. 6. Relation between the bulk modulus and weighted cationic radius ratio (defined in Equation (1)). Error bars are based on fitting a second-order Birch-Murnaghan equations of state to the pressure-volume data in Fig. 4.

distortions around $U^{5+/6+}$ and Ln^{3+} soften the lattice.

No significant correlation was found between bulk modulus and hyperstoichiometry, which is consistent with the ease of incorporating excess oxygen into the fluorite structure [12]. This is consistent with previous experimental work on UO_{2+x} showing an increase in bend strength upon oxidation [43]. However, previous computational work on UO_{2+x} at high pressure [15] showed, in contrast, that the incorporation of oxygen interstitials lowered the bulk modulus of fluorite structured UO_{2+x}. This incongruence suggests that the effects of lanthanide doping on bulk modulus dominate over the effects of hyperstoichiometry, which is consistent with how lanthanide doping is a more dominant factor than hyperstoichiometry in determining unit cell volume at ambient pressure, as discussed previously.

The linearly decreasing value of B_0 with increasing weighted radius ratio is consistent with previous work finding a linear decrease, as a function of dopant concentration, in a wide variety of elastic properties of Ln-doped UO_2 at ambient conditions [22–26]. Additionally, computational simulations show a reduction of B_0 in Ln-doped UO_2 [41], in agreement with the results reported here. Determining the bulk modulus, an elastic property, of UO_2 upon the addition of lanthanides, a major fission product, is important for understanding the behavior of nuclear fuel. Elastic properties are derived from the atomic scale properties of materials, though they affect behavior at the microscale. For instance, a decrease in bulk means a decrease in fuel stiffness, which is a major factor in pellet cracking due to thermal gradients experienced during reactor operation.

We note that our results differ from experiments conducted on SIMFUEL [44], where increased burnup (*i.e.*, higher concentrations of dopant) led to an increase in B_0. SIMFUEL is very different from Ln-doped UO_2: it contains ~10–20 different dopant elements at total concentrations that reach upwards 20 at. %. Furthermore, these dopant elements incorporate into the UO_2 host through multiple routes, including solid solutions, phase separated oxides, and metallic inclusions.

4. Conclusion

Samples of hyperstoichiometric Ln-doped ($Ln_xU_{1-x}O_{2-0.5x+y}$) were studied using *in situ* synchrotron X-ray diffraction at high pressure. DACs allowed compression of material to ~50–55 GPa. All compositions underwent a high-pressure fluorite-to-cotunnite phase transformation. Transition pressures ranged from 21 to 39 GPa, with the mixed-phase regime extending to the highest pressures studied for all compositions, ~50–55 GPa. There was a strong correlation between a composition's increasing hyperstoichiometry and an increase in transition pressure. This was explained by the greater ease of incorporating oxygen interstitials into the fluorite structure as compared with cotunnite. There was a linear trend between B_0 and doping, which showed that increasing the ionic radius and concentration of the lanthanides caused a decrease in B_0. This is consistent with previous work showing a decrease in the magnitude of elastic properties of Ln-doped UO_2 with increasing dopant concentration. Overall, hyperstoichiometry determined the pressure required to induce a phase transformation, while the lanthanide species and its concentration dictated the material's compressibility.

Acknowledgements

This work was supported as part of “Materials Science of Actinides”, an Energy Frontier Research Center funded by the U.S. Department of Energy (DOE) Office of Science, Basic Energy Sciences (Grant No. DE-SC0001089). X-ray diffraction data were collected at beamlines HPCAT (Sector 16), APS, ANL and 12.2.2, ALS, LBNL. HPCAT operations are supported by DOE-NNSA under Award No. DE-NA0001974 and DOE-BES under Award No. DE-FG02-99ER45775, with partial instrumentation funding by NSF. The APS is a U.S. DOE Office of Science User Facility operated for the DOE Office of Science by ANL under Contract No. DE-AC02-06CH11357. The ALS is supported by the Director, Office of Science, Office of Basic Energy Sciences, of the U.S. DOE under Contract No. DE-AC02-05CH11231. Beamline 12.2.2 is partially supported by COMPRES, the Consortium for Materials Properties Research in Earth Sciences under NSF Cooperative Agreement EAR 1606856. R.I.P. gratefully acknowledges the support of the Carnegie-DOE Alliance Center under cooperative agreement DE-NA0002006. Travel for D.R.R. and S.P. was partially supported by the McGee Research Grant program through Stanford University.

Appendix A. Supplementary data

Supplementary data related to this article can be found at http://dx.doi.org/10.1016/j.jnucmat.2017.04.007.

References

[1] E.A.C. Crouch, Fission-product yields from neutron-induced fission, At. Data Nucl. 19 (1977) 417. Data Tables.

[2] D.R. Olander, Mechanistic interpretations of UO_2 oxidation, J. Nucl. Mater. 252 (1998) 121.

[3] P.G. Lucuta, et al., Microstructural features of SIMFUEL—simulated high-burnup UO_2-based nuclear fuel, J. Nucl. Mater. 178 (1991) 48.

[4] P.G. Lucuta, et al., “Thermal conductivity of SIMFUEL, J. Nucl. Mater. 188 (1992) 198.

[5] H. Matzke, Radiation damage-enhanced dissolution of UO_2 in water, J. Nucl. Mater. 190 (1992) 101.

[6] J.T. White, A.T. Nelson, Thermal conductivity of UO_{2+x} and U_4O_{9-y}, J. Nucl. Mater. 443 (2013) 342.

[7] X.Y. Liu, et al., Molecular dynamics simulation of thermal transport in UO_2 containing uranium, oxygen, and fission-product defects, Phys. Rev. Appl. 6 (2016) 044015.

[8] D. Shin, T.M. Besmann, Thermodynamic modeling of the $(U,La)O_{2\pm x}$ solid solution phase, J. Nucl. Mater. 433 (2013) 227.

[9] F.N. Skomurski, et al., Charge distribution and oxygen diffusion in hyperstoichiometric uranium dioxide UO_{2+x} ($x \leq 0.25$), J. Nucl. Mater. 434 (2013) 422.

[10] J. Wang, et al., Average structure and local configuration of excess oxygen in UO_{2+x}, Sci. Rep. 4 (2014) 4216.

[11] B.T.M. Willis, The defect structure of hyper-stoichiometric uranium dioxide, Acta Crystallogr. Sect. A 34 (1978) 88.

[12] P.V. Nerikar, et al., Thermodynamics of fission products in $UO2\pm x$, J. Phys. Condens. Matter 21 (2009) 435602.

[13] U. Benedict, et al., X-ray powder diffraction study of the high pressure behaviour of uranium dioxide, J. Phys. Lett. 43 (1982) 171.

[14] M. Idiri, et al., Behavior of actinide dioxides under pressure: UO_2 and ThO_2, Phys. Rev. B 70 (2004) 014113.

[15] J. Wang, et al., Electronic structure and stability of hyperstoichiometric UO_{2+x} under pressure, Phys. Rev. B 88 (2013) 024109.

[16] I.J. Fritz, Elastic properties of UO_2 at high pressure, J. App. Phys. 47 (1976) 4353.

[17] M. Sanati, et al., Elastic constants, phonon density of states, and thermal properties of UO_2, Phys. Rev. B 84 (2011) 014116.

[18] B.T. Wang, et al., Phonon spectrum, thermodynamic properties, and pressure-temperature phase diagram of uranium dioxide, Phys. Rev. B 88 (2013) 104107.

[19] J.B. Wachtman, et al., Elastic constants of single crystal UO_2 at 25°C, J. Nucl. Mater. 16 (1965) 39.

[20] R.L. Williamson, et al., Multidimensional multiphysics simulation of nuclear fuel behavior, J. Nucl. Mater. 423 (2012) 149.

[21] H. Matzke, et al., Materials research on inert matrices: a screening study, J. Nucl. Mater. 274 (1999) 47.

[22] K. Kurosaki, et al., Nanoindentation studies of UO_2 and $(U,Ce)O_2$, J. Alloys Compd. 381 (2004) 240.

[23] K. Kurosaki, et al., Effect of Nd and Pr addition on the thermal and mechanical properties of $(U,Ce)O_2$, J. Nucl. Mater 389 (2009) 85.

[24] K. Yamada, et al., Study of the thermodynamic properties of $(U,Ce)O_2$, J. Nucl. Mater. 247 (1998) 289.

[25] S. Yamanaka, et al., Mechanical properties of (U,Ce)O2 with and without Nd or Zr, J. Alloys Compd. 327 (2001) 281.

[26] S. Yamanaka, et al., Thermal and mechanical properties of $(U,Er)O_2$, J. Nucl. Mater. 389 (2009) 115.

[27] L. Zhang, A. Navrotsky, Thermochemistry of rare earth doped uranium oxides $Ln_xU_{1-x}O_{2-0.5x+y}$ (Ln= La, Y, Nd), J. Nucl. Mater. 465 (2015) 682.

[28] H.K. Mao, et al., Calibration of the ruby pressure gauge to 800 kbar under quasi-hydrostatic conditions, J. Geophys. Res. Solid Earth 91 (1986) 4673.

[29] S. Klotz, et al., Hydrostatic limits of 11 pressure transmitting media, J. Phys. D. Appl. Phys. 42 (2009) 075413.

[30] C. Prescher, V.B. Prakapenka, DIOPTAS: a program for reduction of two-dimensional X-ray diffraction data and data exploration, High. Press. Res. 35 (2015) 223.

[31] L. Lutterotti, et al., MAUD (material analysis using diffraction): a user friendly Java program for Rietveld texture analysis and more, IUCr Newsl. CPD 21 (1999) 14.

[32] S. Gréaux, et al., Structural characterization of natural UO_2 at pressures up to 82 GPa and temperatures up to 2200 K, Am. Mineral. 93 (2008) 1090.

[33] L. Desgranges, et al., What is the actual local crystalline structure of uranium dioxide, UO2? A new perspective for the most used nuclear fuel, Inorg. Chem. 56 (2017) 321.

[34] J. Shamblin, et al., Probing disorder in isometric pyrochlore and related complex oxides, Nat. Mater. 15 (2016) 507.

[35] B.E. Schaner, Metallographic determination of the UO_2-U_4O_9 phase diagram, J. Nucl. Mater. 2 (1960) 110.

[36] L. Lynds, et al., X-Ray and density study of nonstoichiometry in uranium oxides, Adv. Chem. 39 (1963) 58.

[37] F.X. Zhang, et al., High pressure phase transitions and compressibilities of $Er_2Zr_2O_7$ and $Ho_2Zr_2O_7$, Appl. Phys. Lett. 92 (2008) 011909.

[38] F. Birch, Finite elastic strain of cubic crystals, Phys. Rev. 71 (1947) 809.

[39] T. Le Bihan, et al., Structural behavior of α-uranium with pressures to 100 GPa, Phys. Rev. B 67 (2003) 134102.

[40] P.R. Scott, et al., High-pressure synchrotron X-ray diffraction study of the pyrochlores: $Ho_2Ti_2O_7$, $Y_2Ti_2O_7$ and $Tb_2Ti_2O_7$, High. Press. Res. 31 (2011) 219.

[41] R.K. Behera, et al., Effect of the substitution of f-electron elements on the structure and elastic properties of UO_2, J. Nucl. Mater. 433 (2013) 504.

[42] R.D. Shannon, Revised effective ionic radii and systematic studies of inter-atomic distances in halides and chalcogenides, Acta Crystallogr. Sect. A 32 (1976) 751.

[43] R. Scott, et al., The plastic deformation of uranium oxides above 800 C, J. Nucl. Mater. 1 (1959) 39.

[44] M.C. Pujol, et al., Bulk and Young's modulus of doped UO_2 by synchrotron diffraction under high pressure and Knoop indentation, J. Nucl. Mater. 324 (2004) 189.